International Journal of Mass Spectrometry 289 (2010) 108–118

Contents lists available at ScienceDirect

International Journal of Mass Spectrometry

journal homepage: www.elsevier.com/locate/ijms

Experimental investigation of the ionization mechanisms of uranium in thermal ionization mass spectrometry in the presence of carbon

M. Kraiem*, K. Mayer, T. Gouder, A. Seibert, T. Wiss, H. Thiele, J.-P. Hiernaut

European Commission – Joint Research Centre, Institute for Transuranium Elements, P.O. Box 2340, 76125 Karlsruhe, Germany

ARTICLE INFO

Article history:
Received 18 May 2009
Received in revised form
30 September 2009
Accepted 1 October 2009
Available online 9 October 2009

Keywords:
Uranium
TIMS
Carbon
Uranium carbide

ABSTRACT

Thermal ionization mass spectrometry (TIMS) is a well established instrumental technique for providing accurate and precise isotope ratio measurements of elements with reasonably low first ionization potential. In nuclear safeguards and in environmental research, it is often required to measure the isotope ratios in small samples of uranium. Empirical studies had shown that the ionization yield of uranium and plutonium in a TIMS ion source can be significantly increased in the presence of a carbon source. But, even though carbon appeared crucial in providing high ionization yields, processes taking place on the ionization surface were still not well understood. This paper describes the experimental results obtained from an extended study on the evaporation and ionization mechanisms of uranium occurring on a rhenium mass spectrometry filament in the presence of carbon. Solid state reactions were investigated using X-ray photoelectron spectroscopy (XPS) and scanning electron microscopy (SEM). Additionally, vaporization measurements were performed with a modified-Knudsen cell mass spectrometer for providing information on the neutral uranium species in the vapor phase. Upon heating, under vacuum, the uranyl nitrate sample was found to turn into a uranium carbide compound, independent of the type of carbon used as ionization enhancer. With further heating, uranium carbide leads to formation of single charged uranium metal ions and a small amount of uranium carbide ions. The results are relevant for a thorough understanding of the ion source chemistry of a uranyl nitrate sample under reducing conditions. The significant increase in ionization yield described by many authors on the basis of empirical results can be now fully explained and understood.

1. Introduction

During the last years, much effort has been put into the development of competences and equipment enabling the analysis of very small quantities of material. A specific application of trace amounts analysis refers to the measurement of isotope abundance ratios of plutonium and uranium, including the minor isotopes, which are key signatures of the nuclear-related activities in a State. In the context of a strengthened safeguards system, environmental sampling has proven to be a powerful tool, introduced for discovering undeclared nuclear activities [1–6]. One of the major analytical challenges, however, is related to the small amounts of uranium and plutonium present in such samples. Hence, the measurements are often carried out very close to the instrumental detection limits. Thermal ionization mass spectrometry (TIMS) with samples loaded on metallic filaments (e.g., rhenium) is a well established technique for providing accurate and precise isotope ratio measurements [7]. Moreover, TIMS has profited during the last years from significant instrumental improvements on the detection side (i.e., the multiple ion counting devices) that allowed a down-scaling of the sample size [8–15]. However, the ionization efficiency (ratio of U^+ ions detected vs U atoms loaded on the filament) is very low. In fact, best reported TIMS efficiencies for Pu and U are 1–2% and 0.1%, respectively. Thus, any increase in ionization efficiency will result in a higher analytical sensitivity allowing the sample size to be reduced. Moreover, as the major uncertainty component in the final result originates from counting statistics, improved ionization efficiency results also in a reduced measurement uncertainty. Over the past decades, different empirically developed procedures that help increasing the ionization efficiency of uranium have been extensively described and revealed the positive effect of carbon as ionization enhancer [16–21]. This effect has been ascribed to the reduction of the sample to a chemical form in which metal ions U^+ are easily produced at the expense of the volatile oxide species (e.g., UO^+ and $UO_2{}^+$)—a large fraction of the sample molecules are lost before the filament surface ionization is hot enough to dissociate the molecules and ionize the atoms. Besides its reducing properties, carbon was also found to dissolve into rhenium to form a metal–carbon solid solution [22,23] with an enhanced electron

* Corresponding author. Present address: European Commission – JRC, Institute for Reference Materials and Measurements, Retieseweg 111, B-2440 Geel, Belgium.
E-mail address: monia.kraiem@ec.europa.eu (M. Kraiem).

1387-3806/$ – see front matter © 2009 Elsevier B.V. All rights reserved.
doi:10.1016/j.ijms.2009.10.001

work function, which resulted in a more efficient ion production compared to that of pure rhenium [24–26]. This expectation is not surprising in view of the exponential dependence of the ion yield on the electron work function of the filament material, the ionization potential of the element and the temperature expressed by the Saha–Langmuir equation [27,28].

From the beginning of the 1960s, important works have theorized the formation of a uranium carbide species to explain the enhanced emission of the U^+ metal ions associated with the use of carbon as a reducing agent [16,19,20,29–31]. Although this theory has commonly been accepted, evidence of such a species on the filament surface has not been experimentally proven. The present study aimed at clarifying the evaporation and ionization mechanisms involved in a TIMS measurement of uranium under reducing conditions. To this end, surface analysis techniques such as X-ray photoelectron spectroscopy (XPS) and scanning electron microscopy (SEM) and the modified-Knudsen cell mass spectrometry (KCMS) were employed for characterising the sample behaviour under the same conditions than those occurring in a TIMS ion source. Goals focus respectively on (i) identifying U-compounds formed on the filament surface, (ii) observing changes in the sample morphology during thermal heating, and (iii) studying the neutral and charged U-species evaporating from the filament surface. From the collected data, the main species involved in the thermal evaporation and ionization processes of uranium were identified, giving thus a contribution for a better understanding of the physico-chemical phenomena governing the filament chemistry. The results of the experimental investigations are presented hereafter.

2. Experimental

Solid state reactions on the filament surface were investigated using SEM and XPS techniques. The molecular and atomic species evaporated from the filament surface were identified by means of the modified-Knudsen cell mass spectrometry. All the experimental parameters were selected to simulate the thermal and non-equilibrium conditions occurring in a TIMS ion source. In the present work, the modified-KCMS technique has proven to be a powerful tool for making a comprehensive study of the vapor phase composition above the U–C–Re ternary system. A detailed description of all the experimental procedures is given hereafter.

3. Sample loading procedure

The sample loading procedure represents a fundamental stage for maximisation of ionization efficiency in the ion source of the mass spectrometer. Zone-refined rhenium filaments were firstly pre-degassed for 20 min at some 2100 K and a pressure of $\leq 10^{-6}$ mbar. For filament carburisation, three different types of carbon sources were studied: (i) collodion solution mixed with absolute ethanol in the 1/10 ratio, depositing 2 μl of solution on the filament surface allowed to dry in air at room temperature under a laminar flow bench, (ii) colloidal suspension of graphite (aquadag), depositing 2 μl of suspension on the filament, drying at 350 K in air under a laminar flow bench, and (iii) graphite film sputtered onto the degassed rhenium filament using an E5200 vacuum sputter deposition unit (Polaron Equipment LTD). As any variation of the graphite film thickness might affect the ionization efficiency – and thus the emission of U^+ metal ions – sputtering conditions were kept under control by fixing parameters such as deposition time, current, voltage and pressure. After carburisation, 100 pg of uranium were loaded on the filament as nitrate solution (1 M HNO_3). In the present work, uranium standard reference solutions were prepared by dissolution of EC-101 high purity uranium metal (Institute for Reference Materials and Measurements, Geel, Belgium) in nitric acid 8 M (Merck, Germany). The uranium concentration was adjusted to the desired value by dilution with ultrapure water UHQPS (Millipore, Eschborn, Germany). All the reagents used in our investigations were of Suprapure grade. After U sample loading, the filaments were gently heated in air at 0.8 A, and then taken for a few seconds near red heat.

4. Scanning electron microscopy

The surface of the various samples was investigated by scanning electron microscopy at different magnifications. The samples were prepared according to the loading procedure previously described. The rhenium ribbons were then carefully removed from the filament holders and fixed on carbon planchets for SEM analysis. As needed for SEM analysis, rhenium surfaces were electrically conductive and did not require any further treatment. The SEM (Tescan Vega, Model TS5130 LS), equipped with both secondary electron (SE) and backscattered electron (BSE) detectors, was operated at 30 kV electron beam accelerating potential and 50 μA beam current under an ultra-high vacuum of 10^{-8} mbar. Thermal structural changes were deduced by observing the sample before and after heating ($T > 1000\,^{\circ}C$). The heating was performed in the preparation chamber of the XPS Omicron machine described below. The filaments were subsequently transferred into the SEM and systematically scanned to locate uranium-rich regions for phase identification. Semi-quantitative information on the elemental composition was obtained from energy dispersive X-ray (EDX) microanalysis.

5. X-ray photoelectron spectroscopy

In this work, the XPS technique was used to provide information on the chemical composition of the TIMS filament surface, comprising the graphite coating, the uranium deposit and the rhenium filament material. The analyses were carried out with an Omicron EA125 X-ray photoelectron spectrometer operated under ultra-high vacuum conditions of 10^{-10} mbar. Approximately 2 μg of uranium were loaded on the pre-degassed rhenium filaments according to the procedure described above. The filament carrying the sample was removed from the filament holder (as reported for SEM sample preparation) and then spot-welded by one end onto the XPS sample holder made of tantalum (Fig. 1). The measurement area, below the filament, was covered by a silicon plate. Silicon was chosen because its photoemission lines do not interfere with the photoemission lines of the elements under investigation. During sample handling, care was taken to avoid any filament distortion susceptible to compromise the outcome of the experiments. Sample heating (in intervals of 60–90 s) was carried out in the preparation chamber of the instrument by resistive heating of the filament. For that purpose, the free end of the filament was contacted via an internal electrode to a low voltage power-supply (about 20 V/10 A). The sample temperature was determined using

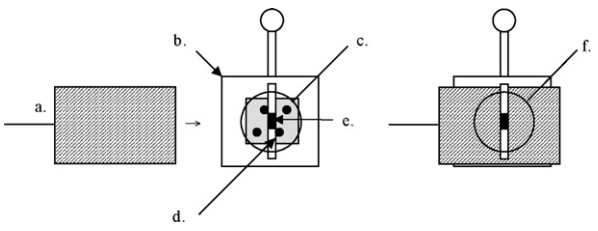

Fig. 1. Shield plate setup to remove the U parasite signal (sight from above): (a.) steel cover; (b.) XPS sample holder made of tantalum; (c.) area exposed to the XPS source; (d.) rhenium filament; (e.) U deposit; and (f.) analysed sample area during an XPS experiment, when the shield plate (a.) is slit below the rhenium filament (f.).

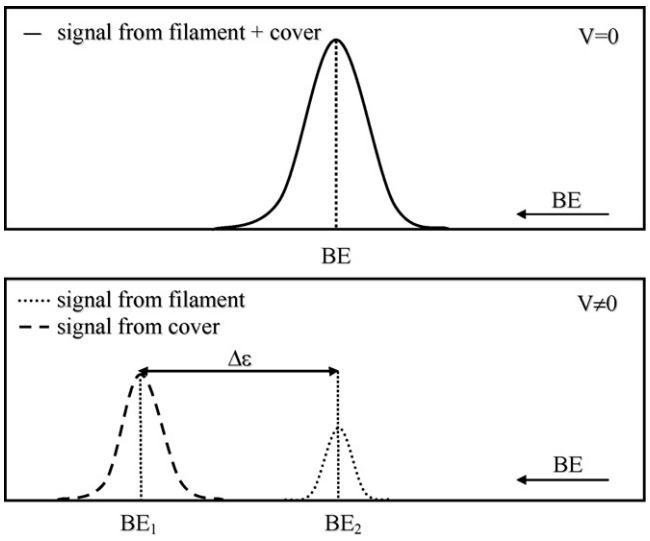

Fig. 2. Separation of the signal contributions arising from cover and filament through the application of a discriminating potential *V* on the cover surface.

an optical pyrometer, deducing the temperature from the filament brightness. A temperature gradient of 373 K over the TIMS filament occurred due to local heat losses at the filament/sample holder and the filament/electrode contact points. Consecutive heating steps were carried out during a single experiment, bringing the filament temperature gradually up to 2073 K – corresponding to the thermal ionization temperature of uranium – to reveal the gradual changes in surface chemistry and composition. Each step was followed by an XPS analysis. Due to varying filament geometry and slight distortions during heating, the sample position had to be adjusted before each XPS run, to ensure that the uranium deposit was well centred in the analysis area, thus producing intense uranium signals. One major experimental difficulty arose from the deposition of volatile uranium species, emitted during heating, on the silicon plate below the TIMS filament. The XPS signal from these deposits had to be removed from the spectrum to ensure a correct interpretation of the solid state reactions occurring on the filament surface. For this purpose, the analysis chamber was equipped with a steel plate, which could be slit between the filament and the Si base plate (see Fig. 1). This plate is free of uranium deposit, because it is not exposed to the filament during heating. It suffers, however, from the drawback that some of the elements under investigation, such as carbon or oxygen, are also found in the plate, thus interfering with the respective photoemission lines of the sample. The lines could still be removed, by simply floating the plate to a potential *V*, resulting in a shift of $e \times V$ of all photoemission lines from the plate. In contrast, the photoemission lines originating from the filament are unaffected by *V* and thus exhibit peaks with unmodified binding energy values (see Fig. 2). This steel plate played a fundamental role for revealing the uranium carbide formation on the filament surface. An overview of the different steps preceding a single XPS analysis is shown in the pictures below (Fig. 3).

6. "Modified" Knudsen cell mass spectrometry (KCMS)

6.1. Experimental setup

In thermal ionization mass spectrometry of uranium, different atomic and molecular species are evaporated from the filament surface. The molecular species may dissociate or decompose and the atomic species may be ionized, depending on the thermodynamic conditions. As mentioned above, the best results in thermal ionization mass spectrometry can be obtained with ion currents, i.e., at high ionization yield of the desired species, in the present case U^+. It is therefore essential to minimise competing reactions and the formation of molecular ions or neutral species. To this end, we studied the different species evaporated from the filament surface. The vaporization measurements were carried out combining a quadrupole mass spectrometer (Balzers QMG 420) with a tungsten crucible, which is in fact the bottom of a Knudsen cell placed in a high temperature furnace maintained under ultra-high vacuum. The essential condition to be preserved was allowing the sample to vaporize under Langmuir conditions (i.e., free-molecular regime), which are those occurring in a TIMS ion source. The entire setup, including the high vacuum pumps, is installed in a glove-box under purified nitrogen. Upon heating, the vaporized species of the molecular beam reaching the ion source of the mass spectrometer were bombardment by electrons (with an energy of 40 eV) in order to ionize the neutral species and thus enable their identification. The temperature was measured with an optical pyrometer sighting in a black-body cavity drilled at the bottom of the cell. At 2700 K, the sample (*ca.* 1 mg) was found to totally vaporize.

6.2. Sample preparation

In order to reproduce the reducing conditions of the TIMS ion source, uranium species evaporating from the surface were investigated using a disk of graphite as sample holder. Small aliquots (5 μl) of a uranyl nitrate solution were successively taken with a push-button micropipette and loaded on top of the disk. Each of the U aliquots was gently dried with an infra-red lamp, which kept the temperature constantly below 300 °C. The whole sample was then carefully placed into the cell and introduced in the modified-Knudsen cell for analysis.

7. Results and discussion

7.1. XPS results

Vacuum carbothermic reduction of the solid uranyl nitrate sample was first investigated in the presence of collodion, and the chemical behaviour derived from the uranium (4f), carbon (1s), rhe-

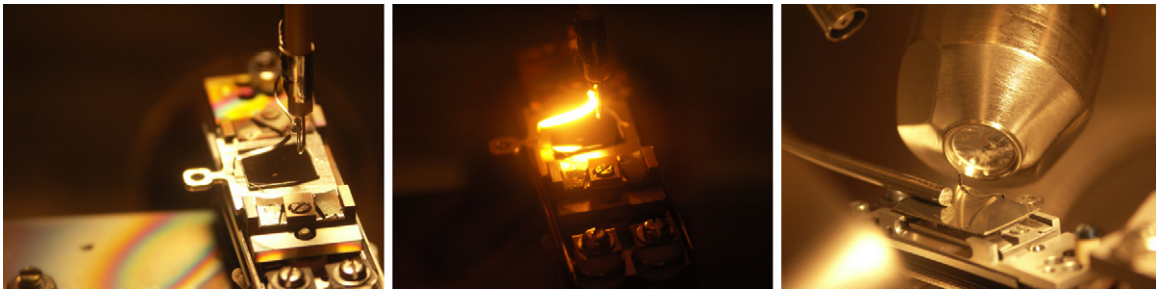

Fig. 3. Sequence of sample heating and irradiation performed on a TIMS filament during an XPS experiment.

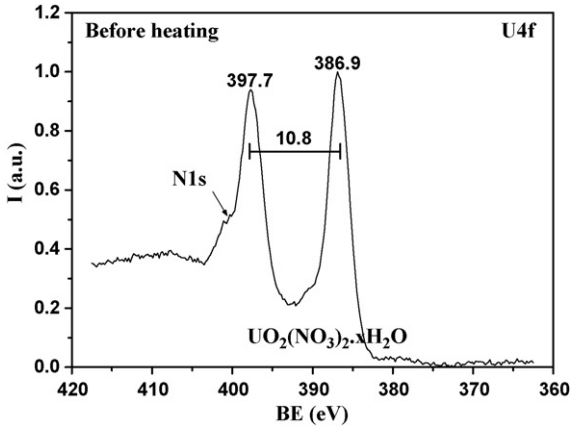

Fig. 4. U4f spectra recorded before sample heating.

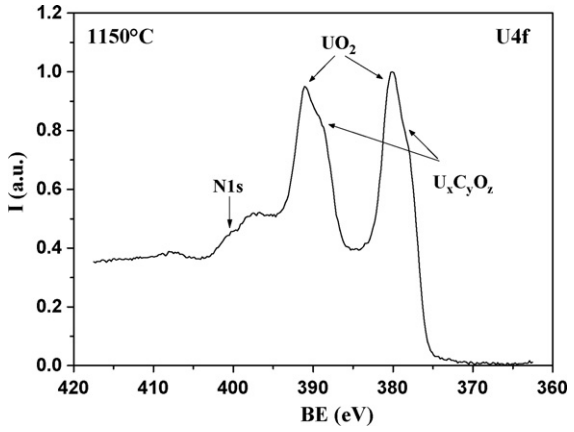

Fig. 5. U4f spectra recorded after sample heating performed at $T = 1150\,^{\circ}C$.

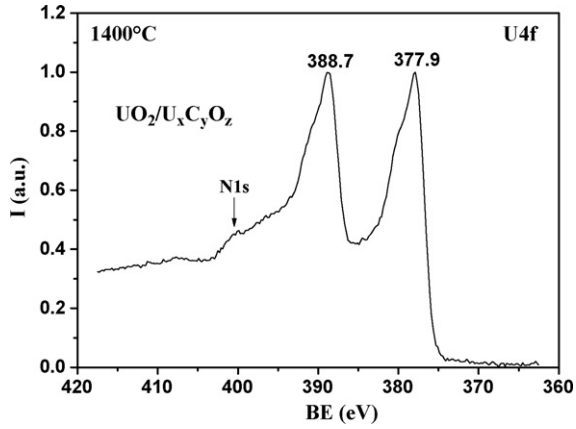

Fig. 6. U4f spectra recorded after sample heating performed at $T = 1400\,^{\circ}C$.

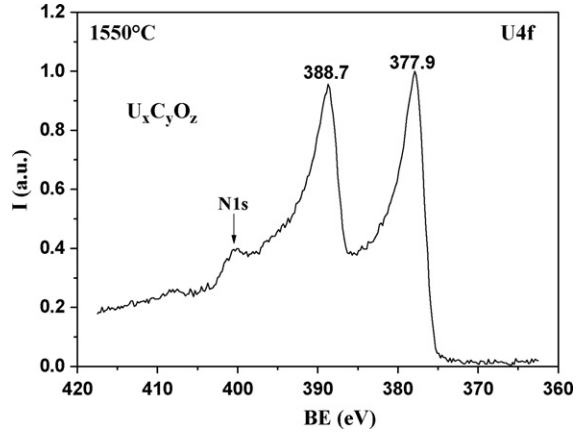

Fig. 7. U4f spectra recorded after sample heating performed at $T = 1550\,^{\circ}C$.

nium (4f) and O (1s) spectra recorded for various heating stages. The initial U4f core level spectrum, obtained prior to sample heating, is reported in Fig. 4. In our sample, consisting in $UO_2(NO_3)_2{\cdot}xH_2O$ (x decreases with the release of hydration water during sample heating), the $U4f_{7/2}$ and $U4f_{5/2}$ photoelectron peaks were observed at abnormally higher binding energies (BE) than those reported by Froideval et al. [32] for similar compounds. These binding energies cannot be explained, even by presence of U^{6+}. They are attributed to surface charging due to the photo-ionization process. In fact, our experimental findings agree quite well with the values obtained by Dash et al. [33] before they applied a correction for charging effects. After heating to 1150 °C, the U4f core levels split into two distinguishable lines, suggesting formation of two different species coexisting on the filament surface (Fig. 5). The first species, with peaks located at higher BE (380.3 and 391.1 eV, respectively), was identified as stoichiometric uranium dioxide, in agreement with literature data. In fact, spectral changes undergoing from UO_2 to UO_{2+x} have been extensively studied and reviewed in the literature [34–54], confirming that the $U4f_{7/2}$ and $U4f_{5/2}$ peaks for UO_2 are sharp and symmetrical, and accompanied by a characteristic shake-up satellite located at +7 eV higher binding energy, i.e., appearing at 397 and 386.7 eV. The U4f peaks at lower BE (388.7 and 377.9 eV, respectively) are attributed to uranium oxycarbide ($U_xC_yO_z$) formed during heating. The experimental values agree well with the reference data reported in Table 1.

After heating to about 1400 °C (Fig. 6), the oxycarbide peaks at lower BE (377.9 and 388.7 eV, respectively) grow at the expense of the uranium dioxide lines and develop an asymmetrical shape, characteristic of uranium carbide. A residual UO_2 component still remains in the U4f core level spectrum. Finally, when filament temperature is thoroughly increased ($T \sim 1550\,^{\circ}C$), carbothermic reduction reaches near completion (Fig. 7). Additional heating does not change the spectrum any further, except for a lowering of the peak intensities due to evaporation of uranium species. The N1s peak at 405 eV, observable in all U4f spectra (Figs. 4–7), is due to nitrogen contained in the loading reagent (uranyl nitrate, nitric acid

Table 1
Comparison between the experimental values and reference data.

Species	$U4f_{7/2}$, BE (eV)	$U4f_{5/2}$, BE (eV)	References
U^0	377.2	388.0	Van den Berghe et al. [53]
	377.6	388.4	Winer et al. [45]
	377.3	388.0	Eckle et al. [55]
$UC_{0.8}$	377.9	388.7	Eckle et al. [55]
UC	377.9	388.7	Dillard et al. [56]; Ejima et al. [57]
$U_xC_yO_z$[a]	377.9	388.7	This work

[a] Such a structure can correspond to a uranium carbide or oxycarbide species.

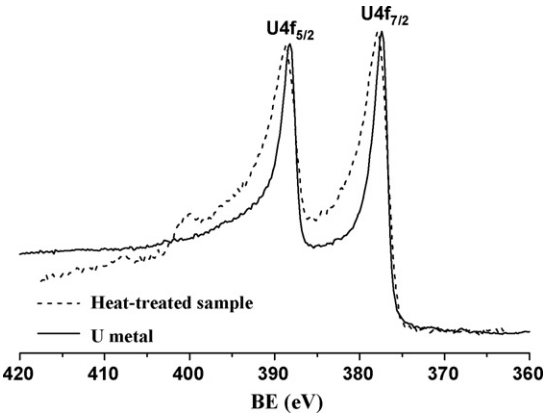

Fig. 8. Comparison of the spectral features for the U carbide and the U metal forms.

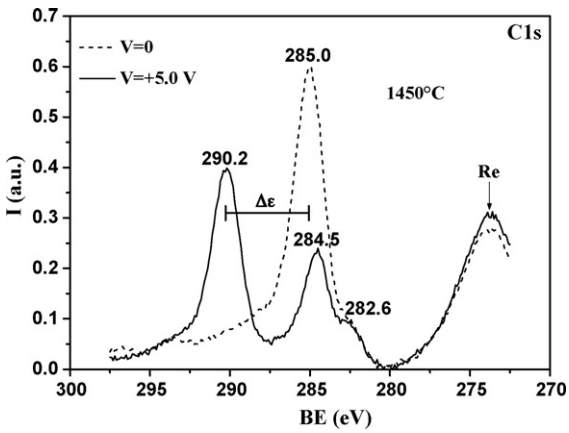

Fig. 9. Evidence of the carbide peak at BE = 282.6 eV in the C1s spectra after sample heating at 1450 °C.

and collodion). This sample impurity was also observed by Pireaux et al. in the XPS studies they conducted on uranyl nitrate powders [39]. But the N1s line resulting from the nitrogen contamination does not perturb the UO_2 shake-up satellites, which are clearly identified.

The U4f binding energies allow attributing the filament surface reactions to the transformation of UO_2 into some uranium carbide species rather than reduction to U metal. The resulting spectrum was found to substantially differ from that of U metal (Fig. 8). U metal peaks, in fact, are sharp and very asymmetrical [58–60], which is in contrast to the spectrum collected from the heat-treated sample. Moreover, the U4f lines show an additional shake-up satellite peak at higher BE, also observed in UC but not in U metal [45,61–63].

Further evidence of the carbide is derived from the C1s core level spectra, which reveal considerable changes in the chemical structure of the carbon present on the filament surface. As extensively described in literature, carbide formation leads to the appearance of a characteristic C1s line around 282 eV BE [55,56,60,64–67]. This line was indeed observed in UC [60]. The C1s spectrum reported in Fig. 9 is, however, dominated by an intense and single broad peak at 285.0 eV (probably due to the convolution of more peaks), and only the presence of a slight shoulder observed in the tail region of this peak might be considered as indication for carbide formation. At this stage of the experiment, great advantage was taken from the use of the cover, allowing to distinguish the filament signal from that of the sample holder, and thus to obtain a carbide line free from interferences. When a potential of +5 V was applied to the shield plate, the main C1s line shifted to 290.2 eV BE. It was then possible to observe a minor but well-defined carbide peak, at 282.6 eV that well, agrees with the reference values reported in Table 2. The second peak, at 284.5 eV, corresponds to the "free" carbon [67–69] resulting from the carbon source introduced on the rhenium filament as ionization enhancer. From these results, it clearly appears that the uranium carbide is formed by the carbothermic reaction between uranium dioxide and carbon being simultaneously present on the filament surface.

Table 2
Reference values for the C1s carbide peak at BE 282 eV.

Species	Binding energy of the electrons 1s for carbon (eV)	References
$U_xC_yO_z$	282.47	Paul and Sherwood [66]
UC_x	281.52	Paul and Sherwood [66]
UC_x ($x = 0.8$)	282.00	Eckle et al. [55]
UC_x ($x > 0.8$)	282.60	Eckle et al. [55]

To confirm that surface carbon is the sole responsible for the disappearance of UO_2, a similar heat treatment was carried on a rhenium/graphite substrate replacing the rhenium/collodion. Formation of the UO_2/oxycarbide mixture was again observed (Fig. 10). In conclusion, the carbon source (collodion, graphite coating or aquadag) had no influence on the reaction as the same products were obtained. However, the carbothermic reduction of UO_2 by aquadag was found to be almost quantitative, i.e., no UO_2 was left. This probably depends on the fact that those filaments carburized with aquadag contained larger amounts of dissolved carbon that thus enabled a better sample reduction.

Because of their similar electronic properties, different carbide species such as UC, UC_2 and U_2C_3, non-stoichiometric carbides

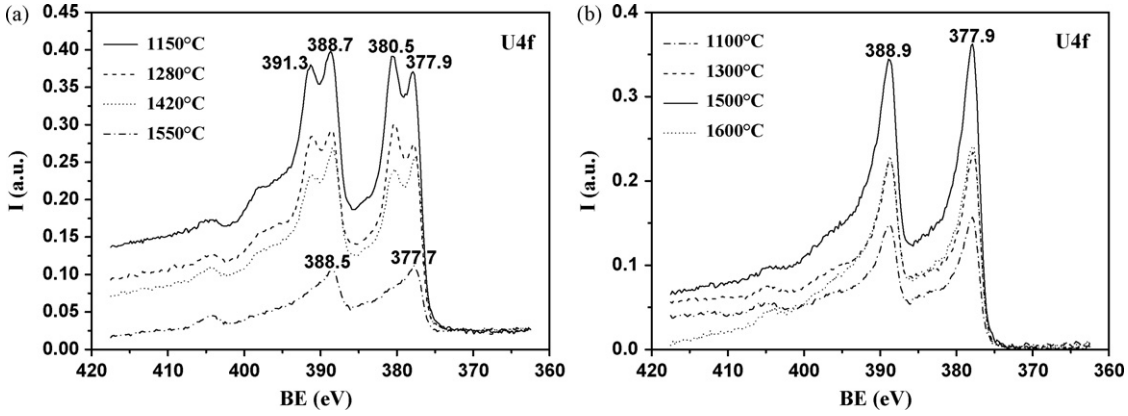

Fig. 10. Evidence of the U sample behaviour at various temperature stages: (a) in the presence of a graphite layer and (b) in the presence of aquadag.

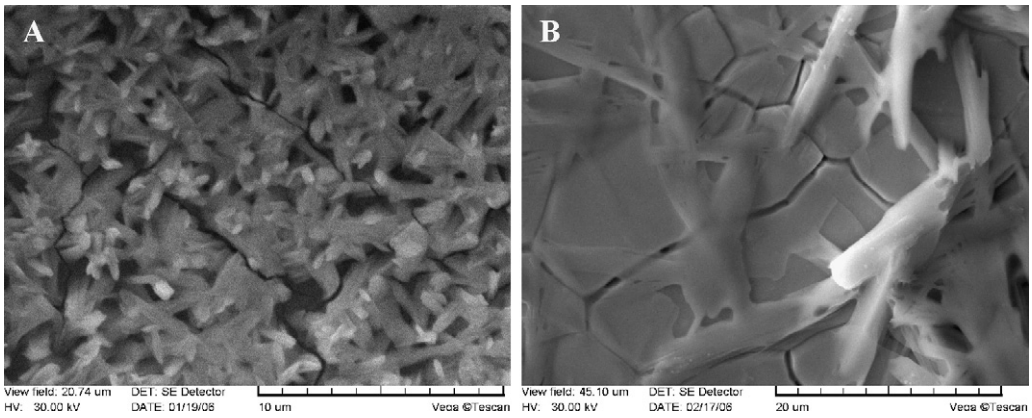

Fig. 11. (A) Boat-shaped and (B) tabular crystal morphologies observed in the samples before heating, and in the presence of carbon.

and oxycarbides have a similar C1s spectrum. Numerous works, in fact, have previously mentioned the difficulty to identify individual carbide species by examining only the XPS and UPS data [55,60]. Usually, a quantitative determination, which consists of the integration of the peaks of interest – U, C and O –, is required for providing the exact stoichiometry of $U_xC_yO_z$. This procedure, however, is affected by the difficult data exploitation due to inhomogeneous surfaces. Sample homogeneity over the entire analysed filament surface is required for obtaining representative elemental (atomic) concentrations. SEM investigations, in fact, revealed that the sample annealing does not meet such requisite but leads to the formation of a non-uniform surface thin layer of oxide and (oxy-)carbide. This is limiting to reliable estimation of the elemental ratios in $U_xC_yO_z$. A second obstacle for correct quantification comes from the low C and O photo-peak intensities, which do not allow a sufficiently accurate evaluation of the corresponding peak areas. Moreover, extra C and O contributions coming from the filament and the sample matrix (e.g., solvent, nitric acid, collodion, etc.) alter the measured area values. Such contributions were found to be hardly controlled even with the use of a blank correction.

Actually, there is still much controversy about which of the uranium carbide species (UC or UC_2) is formed by the carbothermic reduction of uranium dioxide [62,64,68,70–82]. UC_2, however, was reported to be the major reaction product in the presence of a carbon excess. The changes in the oxidation state, responsible for a modified O(1s) photoelectron peak, did not allow revealing the real nature of $U_xC_yO_z$ on the filament surface. However, if we take into account the U–C–O phase diagram in the investigated temperature range together with our operating conditions ($C \gg U$), the uranium oxycarbide and dicarbide appear as the most likely species responsible for the appearance of the carbide peak at 282.6 eV.

7.2. Morphological studies

In the secondary electron imaging (SEI) mode, the bright areas reflect the presence of uranium on the filament surface. From EDX data, U, O and Re appeared as being the major elements present on the filament surface. In all the experiments, the sample behaviour was found to be very similar, independently from the type of carbon source loaded on the TIMS filaments. The SEM images shown in Fig. 11A and B reveal that two different crystal morphologies can be observed on the filament surface prior to heating, respectively composed of: (A) boat-shaped crystals and (B) bladed to tabular crystals. In a few samples, both of these morphologies were found to coexist on the filament surface. With reference to previous works, these crystals were identified as schoepite-type minerals [83–86]. Also called "UO_3 hydrates", these minerals are represented by the general structural formula $UO_3 \cdot (2 \pm x)H_2O$ where $x < 1$ [87]. Chemical nomenclature and crystal morphology for uranyl oxide hydrates of interest are summarised in Table 3.

Schoepite and metaschoepite structures are closely related and only differ by the number of structurally bound H_2O groups [87,88]. In previous works, schoepite was reported to transform slowly in air, at room temperature, to metaschoepite [89–91] and the crystals commonly contain an intergrowth of both these minerals [92]. When subjected to external solicitations (e.g., heat, sunlight, vacuum or mechanical pressure), the remaining schoepite will rapidly transform to dehydrated schoepite $UO_3 \cdot 0.8H_2O$, and this dehydration process was found to be irreversible, with dehydrated schoepite remaining very stable in humid air, even for long periods [87,93]. In water, $UO_3 \cdot 0.8H_2O$ was reported to be stable at near-ambient temperatures, for turning into $UO_3 \cdot 0.9H_2O$ near 100 °C, and then into stoichiometric $UO_3 \cdot H_2O$ above 290 °C [94,95]. Thermal stability fields of schoepite, metaschoepite and dehydrated schoepite were deduced from experimental studies and natural occurrences [87,92]. In this work, it was found that partial dehydration of the starting material $UO_2(NO_3)_2 \cdot 6H_2O$, at nearly 100 °C, leads to formation of schoepite-type minerals on the filament surface. In light of the results, the dependence of the uranyl phases upon the experimental work conditions is not surprising as any variation of the filament current, temperature or either humidity is susceptible to affect the dehydration process. EDX analysis, however, does not enable to solve the stoichiometry of a given phase, due to the complexity of providing the exact value of the oxygen to uranium ratio. From the literature, this ratio was reported to be 5.25 and 5.0, respectively for schoepite and metaschoepite [87,88]. A first obstacle for correct evaluation of such a ratio was ascribed to the fact that the crystals do not consist in a single-phase mineral sample but contain a polycrystalline mixture of schoepite and dehydrated schoepite, which are not distinguishable by EDX analysis. Additionally, a further dehydration of the minerals may occur, under vacuum, after the exposure to the SEM electron beam. Determination of the O to U ratio in the crystal phase is also difficult since other species present on the substrate are responsible for increasing significantly the oxygen content in the sample. These species are HNO_3, collodion and the rhenium oxides produced by surface oxidation with the nitric acid. Note, also, that H cannot be analysed by EDX, which prevents the analyst from the possibility to establish

Table 3
Chemical nomenclature for different uranyl oxide hydrates.

Phase	Chemical formula	Crystal morphology
Schoepite	$[(UO_2)_8O_2(OH)_{12}](H_2O)_{12}$	Orthorhombic, tabular
Metaschoepite	$[(UO_2)_8O_2(OH)_{12}](H_2O)_{10}$	Orthorhombic, tabular
Dehydrated schoepite	$[(UO_2)_4O_{0.25-x}(OH)_{1.5+2x}$	Boat shaped

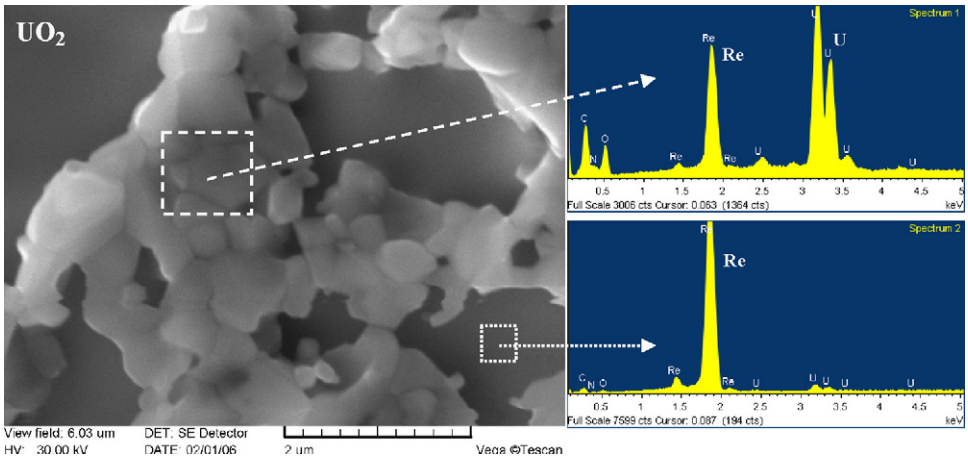

Fig. 12. SEM micrograph showing the UO_2 crystal formation occurring during thermal treatment and EDX analysis of the indicated filament areas.

the exact number of water molecules present in the uranyl oxide hydrate minerals. However, formation of big sized-tabular crystal blocks, as reported in Fig. 11B, may probably be ascribed to the high acidity of the uranyl nitrate solution used in our investigations (HNO_3 = 1 M). Earlier studies, in fact, highlighted the crystals growth to depend on several physico-chemical parameters such as pH, solvent, impurities, over-saturation, etc. and especially the pH was reported to affect the geometry of the crystals (i.e., shape and sizes) [96,97]. After heating, the sample morphology was found to change drastically, and displays near-spherical micrograins that form aggregated clumps with open grain boundaries, as shown in Fig. 12. The morphology of this new mineral phase matches closely with that observed for a UO_2 reference powder [98] whereas it was found to substantially differ from those associated to the higher uranium oxides UO_3, UO_4 and U_3O_8 [99,100]. During the SEM investigations, however the major experimental difficulty was to reveal the uranium carbide formation on the filament surface. Only one sample, in fact, led to a uranium mineral phase characterised by a much lower amount of oxygen (Fig. 13). Referring to the XPS results, this phase was ascribed to a uranium carbide or an oxycarbide. Difficulties for observing optically such a compound may probably be due to its instability by air contact. Prior to SEM analysis, in fact, the samples were briefly exposed to air following the heating stage performed in the Omicron machine. Hence, the uranium carbide film may have re-oxidized to UO_2 during transfer from ultra-high vacuum to air. Moreover, such an ultra-thin layer of uranium carbide might also be responsible for a fast re-oxidation of the sample surface. Maslennikov et al. [101] indicated, in fact, that UC crystallites in air were coated with a thin film of uranium oxycarbide with a C/O ratio of 0.85/0.15. Finally, determination of the C/U ratio was also not helpful as the carbon present on the filament has multiple origins. These are, for instance, the uranium carbide, the ionization enhancer and even the filament substrate itself.

7.3. Evaporated species

As outlined above, the atomic and molecular species evaporated from the filament were investigated using a modified-Knudsen cell. The ion intensity (I_i) of the species i in the cell, at a given temperature T (K), is related to its partial pressure (p_i) by the following equation:

$$p_i = k_i I_i T \tag{1}$$

where k_i is a constant depending on design geometry, ionization conditions and specific properties of the species (i.e., electron ionization cross section and appearance potential). The second law of thermodynamics together with Eq. (1) leads to the following equation used for data evaluation:

$$\sum_i \left(\alpha_i \frac{\mathrm{d}\ln(I_i T)}{\mathrm{d}(1/T)} \right) = -\frac{\Delta H_i^\circ}{R} \tag{2}$$

in which R is the gas constant and α_i the stoichiometric coefficients of the species i.

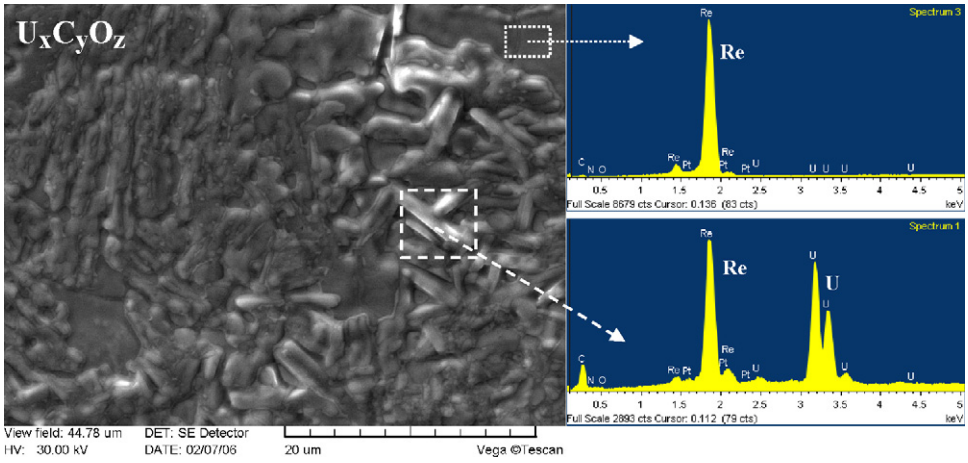

Fig. 13. SEM micrograph showing the uranium carbide formation occurring during thermal treatment and the EDX analysis of the indicated filament areas.

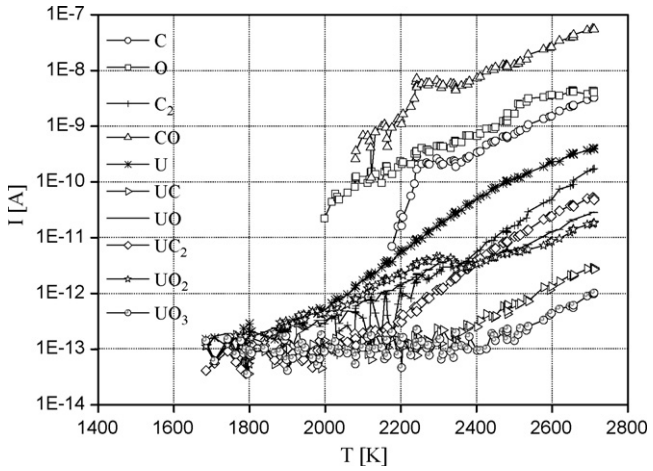

Fig. 14. Logarithmic plot of the evolution of the ion signals for an ionization electron energy of 40 eV.

In the linear region of a $\ln(I_i \times T)$ vs $1/T$ plot, the partial heat of sublimation/evaporation of the species i can be determined from the slope.

Fig. 14 shows the evolution of the mass spectrometer signals of the species in the temperature range of 1700–2750 K. Measurements performed below 1700 K yielded no evidence of MS signals. Above 1800 K, U oxide and carbide ion species were found to gradually increase, and especially U^+ that certainly comes from carbide electron fragmentation, becomes largely predominant.

In the solid phase, the U oxide stoichiometry was evaluated from the oxygen to uranium ratio within the temperature range of 1600–2700 K. This ratio was obtained from a procedure described elsewhere [102], which yields to the following equation:

$$\frac{O}{U} = \frac{3[UO_3] + 2[UO_2] + [UO]}{[UO_3] + [UO_2] + [UO] + [U]} \quad (3)$$

As shown in Fig. 15, UO_2 is found to rapidly turn under heating into hypo-stoichiometric oxide UO_{2-x} for undergoing complete reduction, which is nearby 2400 K. At this temperature, the amount of the U carbide species detected in the vapor phase is also found to increase. It is thus possible to correlate the uranium carbide formation directly with the carbothermic conversion of uranium dioxide, as follows:

$$UO_{2(s)} + 4C_{(gr)} \rightarrow UC_{2(s)} + 2CO_{(g)} \quad (4)$$

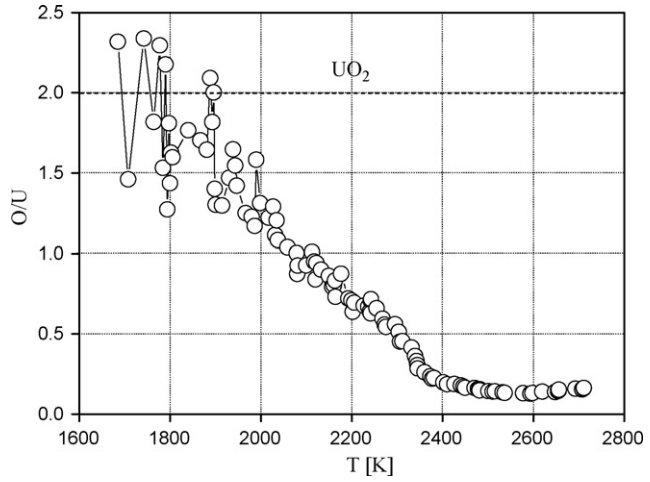

Fig. 15. Dependence of the oxygen to uranium ratio on the absolute temperature.

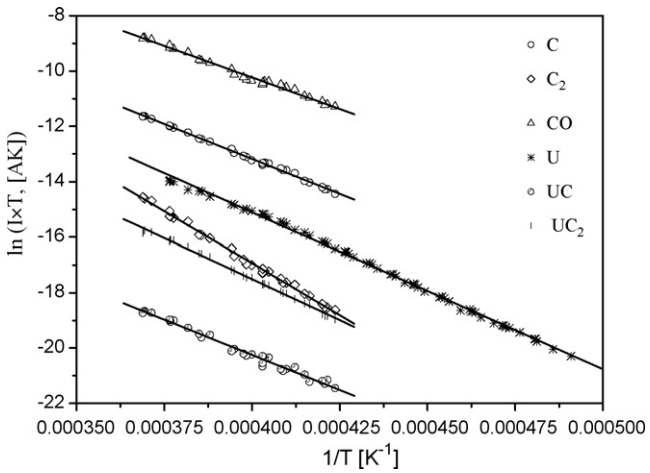

Fig. 16. Arrhenius plot of the measured partial quantity $(I \times T)$ against T^{-1} (K^{-1}) for the uranium carbide species.

Figs. 16 and 17 refer to the experimental data obtained, respectively, for the uranium oxides and carbides. Except for UO and UO_2, one can see that a straight line can be drawn through all the experimental data of the investigated temperature range. For such species, the break of slope at 2350 K suggests that the reaction process is probably made of two distinctive steps. As shown in Table 4, there is a noticeable difference between the experimentally determined partial enthalpies and the published values available for *pure* materials.

Owing to difficulties in obtaining sufficiently accurate thermodynamic data under the current non-equilibrium conditions, it should be emphasized that these data are reliable in the given interpretation context. In the specific case, the behaviour pattern increases in complexity as a chemical *reaction* – involving uranium and graphite arising from the disk – occurs *together* with the vaporization process. For explaining the different rates during the heating procedure, a reaction mechanism including additional steps ((4a)–(4e)) to the previous one is proposed:

$$UO_2 + C \rightleftharpoons UO + CO \quad (4a)$$

$$UO + C \rightleftharpoons U + CO \quad (4b)$$

$$U + C \rightleftharpoons UC \quad (4c)$$

$$UC + C \rightleftharpoons UC_2 \quad (4d)$$

$$C + O \rightleftharpoons CO \quad (4e)$$

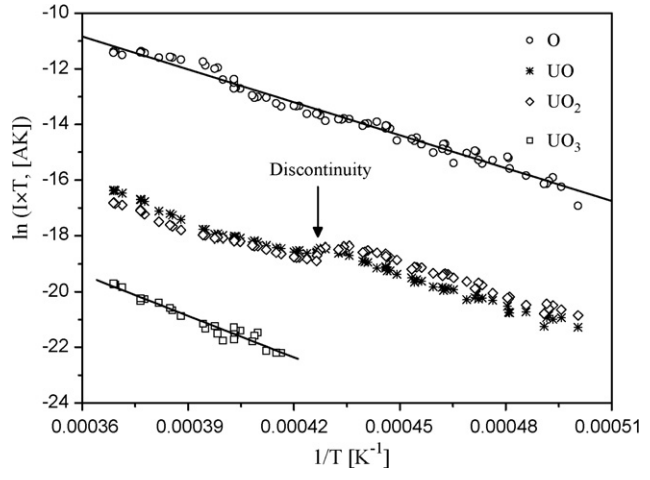

Fig. 17. Arrhenius plot of the measured partial quantity $(I \times T)$ against T^{-1} (K^{-1}) for the uranium oxide species.

Table 4
Experimental and reference partial enthalpies for the carbide species.

Species	ΔT (K)	$\Delta H_{exp.}$ (kcal/mol)	ΔT (K)	$\Delta H_{ref.}$ (kcal/mol)	References
UC_2	2360–2710	117.5 ± 1.3	2000–2500	221.5 ± 0.001	[103]
UC	2360–2710	101.2 ± 2.2			
U	2015–2710	116.9 ± 0.4	2000–2500	128.1 ± 0.0006	[103]
			298	128.1	[104]
C_2	2360–2710	148.8 ± 1.6	2000–2500	188.5 ± 0.0008	[103]
			2500–3500	194.7 ± 0.085	[105]
			2400	199.0 ± 20	[106]
C	2360–2710	100.4 ± 0.9	2000–2500	183.5 ± 0.0008	[103]
			2500–3500	170.6 ± 0.1	[105]
			2400	178.0 ± 10	[106]

Note: the error represents the standard deviation on the slope.

Table 5
Experimental and reference partial enthalpies for the oxide species.

Species	ΔT (K)	$\Delta H_{exp.}$ (kcal/mol)	ΔT (K)	$\Delta H_{ref.}$[a] (kcal/mol)
UO_3	2360–2710	98.9 ± 4.1	1500–2800	157.4 ± 0.5
UO_2	2015–2300	79.7 ± 1.7	1500–2800	140.3 ± 0.5
	2360–2710	73.0 ± 1.8		
UO	2015–2300	79.3 ± 1.9	1500–2800	155.5 ± 0.5
	2360–2710	85.7 ± 2.7		
U	2015–2300	112.0 ± 1.0	1500–2800	180.9 ± 0.4
O	2015–2300	77.8 ± 3.2		
	2360–2710	85.9 ± 4.3		

[a] Species in equilibrium with hypo-stoichiometric uranium dioxide (from the work of Green and Leibowitz [107]).

In this process, conversion of the UO_2 into UC_2 firstly proceeds through generation of UC as an intermediate product, which later gets converted into UC_2.

In literature, the quantity of available carbon was reported to be the limiting step for the UC_2 carbide formation. As a matter of fact, it is not possible to clearly define the final carbide phase composition, which is still matter of debate. However, in the presence of a large excess of carbon – continuously provided by the substrate – it can be assumed that UO_2 converts quantitatively into UC_2. Indeed, the comparable experimental values of the heat of vaporization obtained for UC_2, UC and C reveal more on this concern. In Table 4, these values were reported to be 117.5 ± 1.3, 101.2 ± 2.2 and 100.4 ± 0.9 kcal/mol, respectively. This means that UC^+ forms by electron dissociation of UC_2^+ according to the step

$$UC_2^+ + e^- \rightarrow UC^+ + C^+ + 2e^-, \quad (5)$$

and not directly from $UC_{(s)}$ as it can be expected. On the other hand, the experimental values of C and C_2 are found to substantially differ from the recommended values of $UC_{(s)}$ and C_{gr}, in equilibrium with the respective vapor phases. This means that the graphite disk does not play a role during the evaporation process of the various species. Moreover, the non-linear behaviour observed for UO and UO_2 is most likely due to a major carburisation of $UO_{2(s)}$, which is consistent with the significant MS signal increase observable in Fig. 14 for the corresponding UC and CO reaction products. The experimental uranium partial enthalpy determined from the straight lines – on both sides the discontinuity – well agrees with the value recommended by Green and Leibowitz [107] for the phase equilibrium between $UC_{(g)}$ and the solid (see Table 5). Note in Fig. 16, that the experimental data of the U^+ ions have been reported over an extended temperature range as the intensity of such ions is already appreciable at relatively low temperatures.

Depending on temperature, two mechanisms (6a) and (6b) can be advanced for describing the U metal formation in the vapor phase:

$$UO_{2(s)} + 2C_{(gr)} \rightarrow U_{(g)} + 2CO_{(g)} \quad (6a)$$

$$UO_{2(s)} + 4C_{(gr)} \rightarrow UC_{2(s)} + 2CO_{(g)} \rightarrow UC_{2(g)} \begin{cases} \xrightarrow{e^-} UC^+_{(g)} + 2C^+_{(g)} \\ \xrightarrow{e^-} UC_2{}^+_{(g)} \end{cases} \quad (6b)$$

Mechanism (6a) was found to take place at relatively low temperatures whereas mechanism (6b) preferably occurs for $T > 2300$ K. A mechanism that promotes formation of metal free ions $U_{(vap)}$ from $U_{(s)}$ can also be considered, as

$$UO_{2(s)} + 2C_{gr} \rightarrow U_{(s)} + 2CO_{(g)}. \quad (6c)$$

But this mechanism is not consistent with our previous XPS investigations, during which no metal uranium was found. In fact, they proved uranium dioxide and carbide as being the only species formed on the filament surface. Furthermore, in case that mechanism (6c) would take place on the graphite substrate, a significant U^+ current signal would have been detected earlier during the vaporization measurements, before reaching $T = 2000$ K. According to Ref. [108], the U metal content originated from the carbon reduction of UO_2 was reported to be negligible below 2000 °C, which is in fully agreement with our finding.

At this point, the experimental enthalpy values for U and UC_2 were found to be 116.9 ± 0.4 and 117.5 ± 1.3 kcal/mol, respectively. Such values provide further information on the electron dissociation of UC_2, which occurs in the vapor phase through one of the

following stages:

$$UC_{2(g)}{}^{+} + e^{-} \rightarrow U^{+}{}_{(g)} + 2C^{+}{}_{(g)} + 3e^{-} \quad (7a)$$

$$UC_{2(g)}{}^{+} + e^{-} \rightarrow U^{+}{}_{(g)} + C_2{}^{+}{}_{(g)} + 2e^{-} \quad (7b)$$

As the intensity of the C^+ signal is higher than that of $C_2{}^+$ (see Fig. 14), the above (7a) mechanism appears to describe the preferentially occurring mechanism. However, coexistence of step (7b) with the step (8) reported below can either be responsible for the larger amount of C^+.

$$C_2^+ + e^- \rightarrow 2C^+ + 2e^- \quad (8)$$

8. Conclusion

The mass spectrometric measurements of small amounts of uranium call for measures that increase the ionization yield and thus improve the counting statistics. Reducing agents such as carbon had been empirically found to increase the production of U^+ ions at the expense of molecular ions such as UO^+ in a thermal ionization mass spectrometer. In the present investigation we could experimentally prove the chemical and physico-chemical mechanisms involved from the loading of the filament with uranyl nitrate solution to the formation of uranium ions. The XPS, SEM and modified-KCMS techniques used for investigating the evaporation and ionization processes of uranium in the presence of a carbon source, revealed that upon heating, uranyl nitrate turns into a uranium carbide species which vaporizes from the filament surface mainly as $U_{(vap)}$ or $UC_{2(vap)}$. Such a result was of primary relevance to confirm unambiguously the theory that uranium carbide formation is responsible for the enhancement of the emission efficiency of U^+ ions from the single filament surface ionization source of a mass spectrometer. Moreover, the way in which carbon is made available (coating of the filament surface, addition of graphite suspension or addition of organic solvent) always results in the same mechanisms for ion production. Using graphite as ionization enhancer, greatly increases the ionization yield of uranium and, thus, enables that samples in the sub-picogram range can be analysed for their isotopic composition by thermal ionization mass spectrometry.

References

[1] D.L. Donohue, R. Ziesler, Anal. Chem. 65 (1993) 359A.
[2] E. Kuhn, Environmental monitoring for safeguards applications, in: 36th INMM Annual Meeting Proceedings, Palm Desert, California, 1995.
[3] J.N. Cooley, E. Kuhn, D.L. Donohue, Current status of environmental sampling for IAEA safeguards, in: Proc. 19th Annu. ESARDA Symp. on Safeguards and Nuclear Material Management, Montpellier, France, May 13–15, 1997, pp. 31–35.
[4] J.N. Cooley, IAEA implementation of environmental sampling for safeguards, in: 38th INMM Annual Meeting Proceedings, Phoenix, Arizona, 1997.
[5] D.L. Donohue, J. Alloys Compd. 271 (1998) 11.
[6] D.L. Donohue, Anal. Chem. 74 (2002) 28A.
[7] I.T. Platzner, Modern Isotope Ratio Mass Spectrometry, vol. 145, John Wiley, Chichester, 1997.
[8] S. Richter, S.A. Goldberg, Int. J. Mass Spectrom. 229 (2003) 181.
[9] J.B. Schwieters, C. Bouman, D. Tuttas, M.E. Wieser, Geochim. Cosmochim. Acta 68 (2004) A60.
[10] M.E. Wieser, J.B. Schweiters, Int. J. Mass Spectrom. 242 (2005) 97.
[11] J.B. Schwieters, D. Tuttas, C. Bouman, N. Quaas, Geochim. Cosmochim. Acta 70 (2006) A567.
[12] S. Goldberg, S. Richter, R. Essex, P. Mason, J. Schweiters, IAEA-CN-98/3/07.
[13] S. Richter, A. Alonso, J. Truyens, H. Kühn, A. Verbruggen, R. Wellum, Int. J. Mass Spectrom. 264 (2007) 184.
[14] S. Bürger, L.R. Riciputi, D.A. Bostick, S. Turgeon, E.H. McBay, M. Lavelle, Int. J. Mass Spectrom. 286 (2009) 70.
[15] R. Jakopič, S. Richter, H. Kühn, L. Benedik, B. Pihlar, Y. Aregbe, Int. J. Mass Spectrom. 279 (2009) 87.
[16] M.H. Studier, E.N. Sloth, L.P. Moore, J. Phys. Chem. 66 (1962) 133.
[17] I. Opausky, K.F. Zmbov, Nucl. Sci. 14 (1963) 17.
[18] J.W. Arden, N.H. Gale, Anal. Chem. 46 (1974) 687.
[19] M.H. Kakazu, N.M.P. Moraes, S.S. Iyer, C. Rodrigues, Anal. Chim. Acta 132 (1981) 209.
[20] N. Sasaki, K. Kubo, M. Asano, J. Phys. E: Sci. Instrum. 7 (1974) 386.
[21] D.H. Smith, J.A. Carter, Int. J. Mass Spectrom. Ion Phys. 40 (1981) 211.
[22] G.B. Gaines, C.T. Sims, R.J. Jaffe, J. Electrochem. Soc. 106 (1959) 881.
[23] P.G. Pallmer Jr., R.L. Gordon, M.J. Dresser, J. Appl. Phys. 51 (1980) 3776.
[24] D.H. Smith, J. Chem. Phys. 55 (1971) 4152.
[25] P.G. Pallmer Jr., Ph.D. Thesis, Washington State University, WA, University Microfilms, Ann Arbor, Michigan (1978).
[26] P.G. Pallmer Jr., R.L. Gordon, M.J. Dresser, J. Appl. Phys. 51 (1980) 1798.
[27] I. Langmuir, K.H. Kingdon, Proc. R. Soc. (London) A 107 (1925) 61.
[28] M.J. Dresser, J. Appl. Phys. 39 (1968) 338.
[29] K.F. Zmbov, Nucl. Sci. 13 (1962) 17.
[30] K.F. Zmbov, Dritte Arbeitstagung über Stabile Isotope (1965) 369.
[31] J.M. Kelley, D.M. Robertson, Anal. Chem. 57 (1985) 124.
[32] A. Froideval, M. Del Nero, R. Carillon, J. Hommet, G. Mignot, J. Colloid Interface Sci. 266 (2003) 221.
[33] S. Dash, M. Kamruddin, S. Bera, P.K. Ajikumar, A.K. Tyagi, S.V. Narasimhan, B. Raj, J. Nucl. Mater. 264 (1999) 271.
[34] B.W. Veal, D.J. Lam, Phys. Rev. B: Condens. Matter 10 (1974) 4902.
[35] G.C. Allen, J.A. Crofts, M.T. Curtis, P.M. Tucker, D. Chadwick, P.J. Hampson, J. Chem. Soc., Dalton Trans. (1974) 1296.
[36] J.C. Fuggle, A.F. Burr, L.M. Watson, D.J. Fabian, W. Lang, J. Phys. F: Met. Phys. 4 (1974) 335.
[37] C. Keller, C.K. Jørgensen, Chem. Phys. Lett. 32 (1975) 397.
[38] C. Miyake, H. Sakurai, S. Imoto, Chem. Phys. Lett. 36 (1975) 158.
[39] J.J. Pireaux, J. Riga, E. Thibaut, C. Tenret-Noel, R. Caudano, J.J. Verbist, Chem. Phys. 22 (1977) 113.
[40] Yu.A. Teterin, V.M. Kulakov, A.S. Baev, N.B. Nevzorov, I.V. Melnikov, V.A. Streltsov, L.G. Mashirov, D.N. Suglubov, A.G. Zelenkov, Phys. Chem. Miner. 7 (1981) 151.
[41] L.E. Cox, J. Electron. Spectrosc. Relat. Phenom. 26 (1982) 167.
[42] R.J. Thorn, J. Phys. Chem. Solids 43 (6) (1982) 571.
[43] G.C. Allen, P.M. Tucker, J.W. Tyler, J. Phys. Chem. 86 (1982) 224.
[44] A.S. Baev, Yu.A. Teterin, L.G. Mashirov, D.N. Suglobov, Sov. Radiochem. 28 (1986) 418.
[45] K. Winer, C.A. Colmenares, R.L. Smith, F. Wooten, Surf. Sci. 177 (1986) 484.
[46] G.C. Allen, N.R. Holmes, J. Chem. Soc., Dalton Trans. 12 (1987) 3009.
[47] G.C. Allen, P.A. Tempest, J.W. Tyler, J. Chem. Soc., Faraday Trans. 1 (1987) 925.
[48] J.F. Moulder, W.F. Stickle, P.E. Sobol, K.D. Bomben, in: J. Chastain (Ed.), Handbook of X-Ray Photoelectron Spectroscopy, Perkin-Elmer Corporation Physical Electronics, 1992 (2nd edition).
[49] Yu.A. Teterin, J. Struct. Chem. 39 (1998) 850.
[50] Yu.A. Teterin, V.A. Terechov, A.Yu. Teterin, K.E. Ivanov, I.O. Utkini, A.M. Lebedev, L. Vukchevich, J. Electron. Spectrosc. Relat. Phenom. 96 (1998) 229.
[51] S. Van den Berghe, J.P. Laval, B. Gaudreau, H. Terryn, M. Verwerft, J. Nucl. Mater. 277 (2000) 28.
[52] Yu.A. Teterin, V.A. Terehov, M.V. Ryzhkov, I.O. Utkin, K.E. Ivanov, A.Yu. Teterin, A.S. Nikitin, J. Electron. Spectrosc. Relat. Phenom. 114–116 (2001) 915.
[53] S. Van den Berghe, F. Miserque, T. Gouder, B. Gaudreau, M. Verwerft, J. Nucl. Mater. 294 (2001) 168.
[54] D. Kumar, S. Bera, A.K. Tripathi, G.K. Dey, N.M. Gupta, Microporous Mesoporous Mater. 66 (2003) 157.
[55] M. Eckle, R. Eloirdi, T. Gouder, M. Colarieti Tosti, F. Wastin, J. Rebizant, J. Nucl. Mater. 334 (2004) 1.
[56] J.G. Dillard, H. Moers, H. Klewe-Nebenius, G. Kirch, G. Pfennig, H.J. Ache, J. Phys. Chem. 88 (1984) 4104.
[57] T. Ejima, S. Sato, S. Suzuki, Y. Saito, S. Fujimori, N. Sato, M. Kasaya, T. Komatubara, T. Kasuya, Y. Onuki, T.J. Ishii, Phys. Rev. B: Condens. Matter 53 (1996) 1806.
[58] S. Fujimori, Y. Saito, K. Yamaki, T. Okane, N. Sato, T. Komatsubara, S. Suzuki, S. Sato, Surf. Sci. 444 (2000) 180.
[59] T. Gouder, Surf. Sci. 382 (1997) 26.
[60] T. Gouder, C.A. Colmenares, J.R. Naegele, Surf. Sci. 342 (1995) 299.
[61] J.G. Dillard, H. Moers, H. Klewe-Nebenius, G. Kirch, G. Pfennig, H.J. Ache, Surf. Sci. 145 (1984) 62.
[62] W. McLean, C.A. Colmenares, R.L. Smith, G.A. Somorjai, Phys. Rev. B: Condens. Matter 25 (1982) 8.
[63] S.B. Nornes, R.G. Meisenheimer, Surf. Sci. 88 (1979) 191.
[64] R. Asuvathraman, S. Rajagopalan, K. Ananthasivan, C.K. Mathews, R.M. Mallya, J. Nucl. Mater. 224 (1995) 25.
[65] L.I. Johansson, Surf. Sci. Rep. 21 (1995) 177.
[66] A.J. Paul, P.M.A. Sherwood, Surf. Interface Anal. 10 (1987) 238.
[67] D.T. Larson, J.M. Haschke, Inorg. Chem. 20 (1981) 1945.
[68] B.R.T. Frost, J. Nucl. Mater. 10 (1963) 265.
[69] F.R. McFeely, S.P. Kowalczyk, L. Ley, R.G. Cavell, R.A. Pollak, D.A. Shirley, Phys. Rev. B: Condens. Matter 9 (1974) 5268.
[70] J.D. Farr, E.J. Huber, E.L. Head, C.E. Holley, J. Phys. Chem. 63 (1959) 1455.
[71] B. Craven, E.R. McCartney, J. Am. Ceram. Soc. 44 (1961) 12.
[72] J. Crane, F.B. Litton, H.S. Kalish, ASM Trans. Q 56 (1963) 176.
[73] W. Schüle, P. Spindler, J. Nucl. Mater. 32 (1969) 20.
[74] J. Bečvář, J. Nucl. Mater. 32 (1969) 156.
[75] T.B. Lindemer, M.D. Allen, J.M. Leitnaker, J. Am. Ceram. Soc. 52 (1969) 233.
[76] A. Pialoux, Thèse d'Etat, Paris-Sud, Orsay, 1973.
[77] G. Danger, J. Besson, J. Nucl. Mater. 54 (1974) 190.
[78] A. Pialoux, M. Dode, J. Nucl. Mater. 56 (1975) 221.
[79] T. Gouder, C.A. Colmenares, J.R. Naegele, J.C. Spirlet, J. Verbist, Surf. Sci. 264 (1992) 354.
[80] R.S. Mehrota, Mater. Res. Bull. 28 (1993) 1193.

[81] A.H.M. Evensen, R. Catherall, P.V. Drumm, P. Van Duppen, O.C. Jonsson, E. Kugler, J. Lettry, O. Tengblad, V. Tikhonov, H.L. Ravn, the Isolde Collaboration, Nucl. Instrum. Methods Phys. Res. Sect. B 126 (1997) 160.
[82] J. Greene, P. Decrock, J. Nolen, G. Thomas, W. Talbert, INTDS Newsletter, PHY-8759-HI-97 (1997).
[83] M.E. Torrero, J. Depablo, M.C.A. Sandino, B. Grambow, Radiochim. Acta 66–67 (1994) 29.
[84] A.G. Sowder, S.B. Clark, R.A. Fjeld, Radiochim. Acta 74 (1996) 45.
[85] A. Finn, D.J. Wronkiewicz, R.J. Finch, J.C. Hoh, C. Merlz, J.W. Emery, E.C. Buck, J. Fortner, S.F. Wolf, L.A. Neimark, J.K. Bates, ANL-98/12, Argonne National Laboratory (1998).
[86] C.H. Mattus, L.R. Dole, The 10th International Conference on Environmental Remediation and Radioactive Waste Management, Glasgow, Scotland, 2005, ICEM05-1371.
[87] C.L. Christ, J.R. Clark, Am. Mineral. 45 (1960) 1026.
[88] P.G. Debets, B.O. Loopstra, J. Inorg. Nucl. Chem. 25 (1963) 945.
[89] A. Shoep, S. Stradiot, Am. Mineral. 32 (1947) 344.
[90] R.J. Finch, M.A. Cooper, F.C. Hawthorne, R.C. Ewing, Can. Mineral. 34 (1996) 107.
[91] R. Finch, T. Murakami, Rev. Mineral. Geochem. 38 (1999) 91.
[92] R.J. Finch, F.C. Hawthorne, R.C. Ewing, Can. Mineral. 36 (1998) 831.
[93] J.K. Dawson, E. Wait, K. Alcock, D.R. Chilton, J. Chem. Soc. (1956) 3531.
[94] H.R. Hoekstra, S. Spiegel, J. Inorg. Nucl. Chem. 35 (1973) 761.
[95] P.A.G. O'Hare, B.M. Lewis, S.N. Nguyen, J. Chem. Thermodyn. 20 (1988) 1287.
[96] M. Schindler, A. Putnis, Can. Mineral. 42 (6) (2004) 1667.
[97] J.I. Friese, M. Douglas, B.K. McNamara, S.B. Clark, B.D. Hanson, PNLL-14856, AC06-76RL01830, Pacific Northwest Laboratory, Richland, WA (2004).
[98] Pyrohydrolyse du difluorure d'uranyle, Intervenants: GT1 (M. Debacq, S. Hébrard, F. Patisson, D. Ablitzer), Collaborations: CEA (C. Ablitzer), Cogema (D. Hartmann).
[99] F. Patisson, C. Ablitzer-Thouroude, S. Hébrard, D. Ablitzer in: Congrès "Matériaux 2006", Colloque "maîtrise des microstructures des matériaux", Dijon, France, Nov. 13-17, 2006, ISBN 978-2-9528-1400-3.
[100] S. Chabod, Thèse "Développement et modélisation de chambres à fission pour les hauts flux, mise en application au RHF (ILL) et à Mégapie (PSI)", Université Paris XI (2006).
[101] A. Maslennikov, B. Fourest, V. Sladkov, Ph. Moisy, J. Alloys Compd. 444–445 (2007) 550.
[102] F. Capone, J.-Y. Colle, J.P. Hiernaut, C. Ronchi, J. Phys. Chem. A 103 (1999) 10899.
[103] L. Leibowitz, R. Blomquist, J.K. Fink, P. Finn, D.F. Fischer, D.R. Fredrickson, S.D. Gabelnick, D. Green, J. Heiberger, C. Kim, M. Chasanov, R. Kumar, R. Land, G. Reedy, A. Sheth, F.A. Cafasso, L. Burris, Report ANL 7545, Argonne National Laboratory, Illinois (1975).
[104] F.L. Oetting, J.M. Leitnaker, J. Chem. Thermodyn. 4 (1972) 199.
[105] L.V. Gurvich, I.V. Veyts, C.B. Alcock, Thermochemical Properties of Individual Substances, vols. 1–3, 4th ed., Hemisphere Pub. Corp., New York, 1989, Also see original Russian editions loc. cit., and NIST Special Database 5, "IVTANTHERMO", L.V. Gurvich, V.S. Iorish, D.V. Chekhovsioi, V.S. Yungman, CRC Press, Boca Raton, Florida (1993).
[106] R.E. Honig, J. Chem. Phys. 22 (1954) 126.
[107] D.W. Green, L. Leibowitz, J. Nucl. Mater. 105 (1982) 94.
[108] J.J. Katz, G.T. Seaborg, The Chemistry of the Actinide Elements, John Wiley and Sons Ltd., Toronto, 1957.